Neutron Diffraction from Shear Ordered Colloidal Dispersions

Heiner Versmold

Institut für Physikalische Chemie, Rheinisch-Westfälische Technische Hochschule, D-52062 Aachen, Germany

(Received 10 April 1995)

Small-angle neutron scattering patterns from shear ordered colloidal dispersions are discussed in terms of the scattering power distribution $I(1)$ along Bragg rods of hexagonal layers. The orientation dependence of the neutron scattering pattern is directly related to $I(1)$. Its experimental determination provides information on the structure and on stacking faults in such systems. Experimental data of Laun *et al.* [J. Rheol. **36**, 743 (1992)] are discussed, and it is found that the system considered is close to random close-packed hexagonal layers.

PACS numbers: 82.70.Dd, 61.12.Bt

The equilibrium phase behavior of charge stabilized colloidal dispersions has been investigated as a function of particle concentration and ionic strength [1] by synchrotron x-ray diffraction [2], by light scattering Kossel lines [3], and by computer simulation [4]. There is agreement that at high particle concentration and low ionic strength the equilibrium structure is fcc (or a glass) in the bulk phase.

Small-angle neutron scattering experiments have also been performed with charge stabilized dispersions at high volume fraction and low ionic strength by several groups. Sharp diffraction peaks of hexagonal arrangement have been obtained for samples subjected to shear either at low rates or after turning the shear off [5–8]. Since the equilibrium structure under these conditions is fcc, the observed neutron diffraction pattern has been interpreted as resulting from fcc [5,6]. Recently, however, this interpretation has been criticized and an interpretation in terms of completely uncorrelated hexagonal layers was presented [9]. In this Letter we want to extend our previous arguments and show that conceptually it is advantageous to start from uncorrelated hexagonal layers as the basic structure element. Additional ordering such as close packing and different stacking sequences leads to a redistribution of the intensity along the Bragg rods in reciprocal space, which can be studied uniquely by small-angle neutron scattering. We recall that light scattering powder diffraction patterns from hard sphere colloidal systems have also been interpreted along these lines [10].

The reciprocal space of a hexagonal layer is a system of hexagonally arranged Bragg rods [11] with a rod spacing in reciprocal space of $a^* = 4\pi/a\sqrt{3}$, where a is the lattice constant of the original lattice. Figure 1 shows a system of Bragg rods (h, k). For laterally uncorrelated layers the intensity is uniformly distributed along the rods. Also included in Fig. 1 is the intensity distribution on the rods for perfect $ABCABC\ldots$ stacking of the layers. In this case the original lattice is fcc and the reciprocal lattice bcc. On the Bragg rods the intensity degenerates to points (h, k, l). With a spacing between two close-packed layers $c = a\sqrt{2}/\sqrt{3}$, we have $c^* = 2\pi/c$. There are two types of Bragg rods [11]. If $(h - k) = 3n$, where n is an integer, reciprocal lattice points occur on the rods at integral values of l. This does not only hold for fcc but also for all other stacking sequences, as long as the layers are snapped in A, B, or C positions. In Fig. 1 the central rod and the six outermost rods are of this type and the corresponding intensity nodes are shown. On the other hand, if $(h - k) = 3n \pm 1$, intensity nodes occur for fcc alternatively at $l + \frac{1}{3}$ or $l - \frac{1}{3}$ with l integral. In Fig. 1 the inner ring with six Bragg rods is of this type. Again the reciprocal lattice points are included. As a guide to the eye a reciprocal bcc unit cell is also shown. For hcp, $ABAB\ldots$ stacking, on each of the latter rods intensity is found at integer l and at $l + \frac{1}{2}$ with an intensity ratio of 1:3 [11].

Stacking sequences other than $ABCABC\ldots$ and $ABAB\ldots$ may occur. For such cases the probability P_m that two layers separated by $m \cdot c$ are identical can be introduced [11]. For the $(h - k) = 3n$ rods the scattering power $I(l)$ along the rods remains distributed, as discussed above, as long as the layers are snapped in

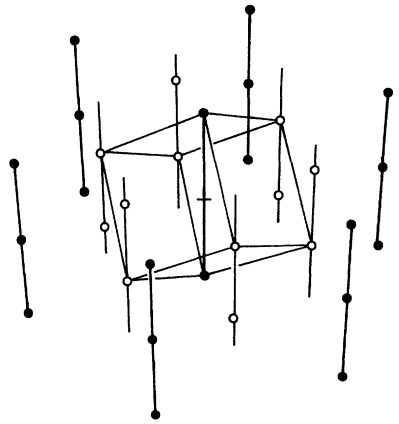

FIG. 1. Bragg rods corresponding to hexagonal layers. For $ABC\ldots$ close-packed layers (fcc) the reciprocal lattice is bcc. The corresponding intensity nodes on the rods and a bcc unit cell are included.

0031-9007/95/75(4)/763(4)$06.00

A, B, or C positions. For the $(h - k) = 3n \pm 1$ rods, the intensity distribution depends on the stacking probabilities P_m. Three examples of $I(l)$ calculated according to Ref. [11] are shown in Fig. 2, which correspond to twinned fcc with stacking faults (bottom), to close-packed random stacking (middle), and to hcp with stacking faults (top panel). It is interesting to note that the probabilities P_m are related to the scattering power $I(l)$ along the rods by [11]

$$P_m - \frac{1}{3} \propto \int_0^1 I(l) \exp(-2\pi i l m)\, dl. \qquad (1)$$

Thus, the intensity distribution along the two types of rods can provide two distinct pieces of information. First, the distribution along the $(h - k) = 3n$ rods allows us to estimate to which extent the layers are locked in close-packing positions with respect to each other. Second, experimental measurements of $I(l)$ along the $(h - k) = 3n \pm 1$ rods provide information on the stacking sequence probability P_m.

Next, we discuss how the scattering power $I(l)$ along the rods can be determined by small-angle neutron scattering. Figure 3(a) shows a view from the top on the Bragg rods shown in Fig. 1. Values for the indices (h, k) of the hexagonal arrangement are included. A rotation by 90° about the $(\bar{2}, 1)$-$(0, 0)$-$(2, \bar{1})$ axis brings the Bragg rods in a position parallel to the drawing plane. This is shown in Fig. 3(b) for l ranging from -1 to $+1$. In this projection all (h, k, l) rods with fixed index h are projected on top of each other. It is therefore not possible to distinguish between the $(h - k) = 3n$ and the $(h - k) = 3n \pm 1$ rods in this projection. Arbitrarily, to the right-hand side of the $(0, k, l)$ rods two $(h - k) = 3n$ rods are shown. The indicated nodes correspond to perfectly close-packed hexagonal layers. To the left of the $(0, k, l)$ rods two $(h - k) = 3n \pm 1$ rods are drawn. On these rods the intensity distribution for random close packing (Fig. 2, middle panel) is shown.

A second projection of the Bragg rods is obtained if Fig. 3(a) is rotated by 90° about the (0,1)-(0,0)-(0, $\bar{1}$) axis. The resulting top view on the Bragg rods is depicted in Fig. 3(c). This time the $(h - k) = 3n$ and the $(h - k) = 3n \pm 1$ rods are separated. The intensity distribution on the $(h - k) = 3n$ rods is chosen as before. For the $(h - k) = 3n \pm 1$ rods in the lower half of Fig. 3(c) the intensity distribution $I(l)$ corresponding to random close packing and in the upper half $I(l)$ for twinned fcc with faults is shown.

With a neutron wavelength $\lambda \approx 10.0 \times 10^{-10}$ m and a lattice constant of $a \approx 1 \times 10^{-6}$ m, the radius of the Ewald sphere $2\pi/\lambda$ is about 3 orders of magnitude larger

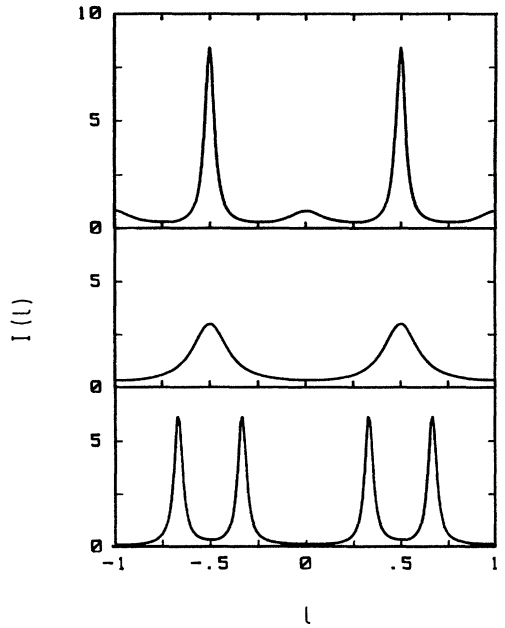

FIG. 2. Scattering power distribution $I(l)$ along the rods $(h - k) = 3n \pm 1$ rods for fcc with stacking faults (bottom), random packing (middle), and hcp with stacking faults (top panel).

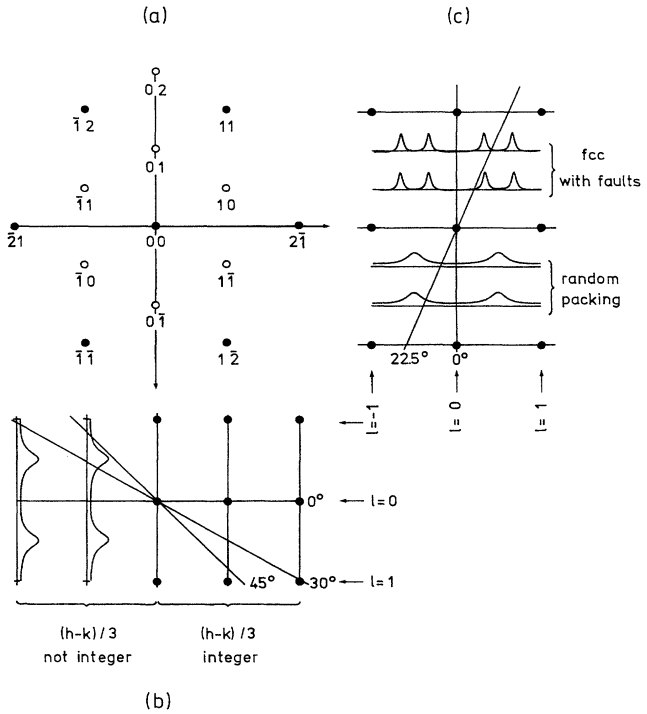

FIG. 3. (a) Top view on an indexed hexagonal layer. (b) Layer in (a) rotated by 90° about the $(\bar{2}, 1)$-$(0, 0)$-$(2, \bar{1})$ axis. Right-hand side: intensity distribution $I(l)$ along $(h - k) = 3n$ rods for close-packed systems. Left-hand side: $I(l)$ along the $(h - k) = 3n \pm 1$ rods for random close packing. (c) Layer in (a) rotated by 90° about the (0,1)-(0,0)-(0, $\bar{1}$) axis. $I(l)$ for $(h - k) = 3n$ rods as in (b). $(h - k) = 3n \pm 1$ rods: $I(l)$ for faulted fcc is shown in the upper part and $I(l)$ for random close packing in the lower part.

than the Q_{hkl} distances in the reciprocal lattice, i.e., on the scale of the reciprocal lattice the Ewald sphere is a plane. For a neutron beam at normal incidence to the hexagonal layers the Ewald plane appears as a line at $l = 0$ in the two projections, Fig. 3(b) and 3(c). From the upper part of Fig. 3(c) it is obvious that for fcc only the $(h - k) = 3n$ rods have intensity nodes in the Ewald plane at normal incidence.

Hexagonal neutron diffraction pattern from colloidal dispersions have been obtained by several groups for dispersions under sheared conditions at low shear rate or after the shear was turned off [5–7]. We consider data published by Laun *et al.* [7]. Typical diffraction patterns, redrawn after Fig. 21 of Ref. [7], are shown in Figs. 4(a)–4(c). The data were obtained at a wall shear rate 10^{-4} s^{-1} in a plane Poiseuille cell with flow in the $(\bar{2}, 1)$-$(0, 0)$-$(2, \bar{1})$ direction (particle diameter σ = 165 nm, solid content 52.3 vol%, dispersed in glycol). These scattering distributions are of particular interest because they were obtained at various orientations of the cell with respect to the neutron beam. To the best of our knowledge the orientation dependence of the scattering distributions has not been accounted for so far.

The diffraction pattern in Fig. 4(a), which was obtained with the neutron beam perpendicular to the layers, shows intensity not only on the $(h - k) = 3n$ rods (1,1), $(2, \bar{1})$, $(1, \bar{2})$, $(\bar{1}, \bar{1})$, $(\bar{2}, 1)$, and $(\bar{1}, 2)$ but also on the $(h - k) = 3n \pm 1$ rods (0,1), (1,0), $(1, \bar{1})$, $(0, \bar{1})$, $(\bar{1}, 0)$, and $(\bar{1}, 1)$. Thus, according to the discussion above [Fig. 3(c) upper part], this structure is *not* fcc as claimed previously [5,6]. However, for hcp as well as for random packed layers the intensity on the $(h - k) = 3n \pm 1$ rods does not vanish in the Ewald plane (line at $l = 0$). Thus, these structures as well as laterally uncorrelated layers are in agreement with the scattering distribution in Fig. 4(a).

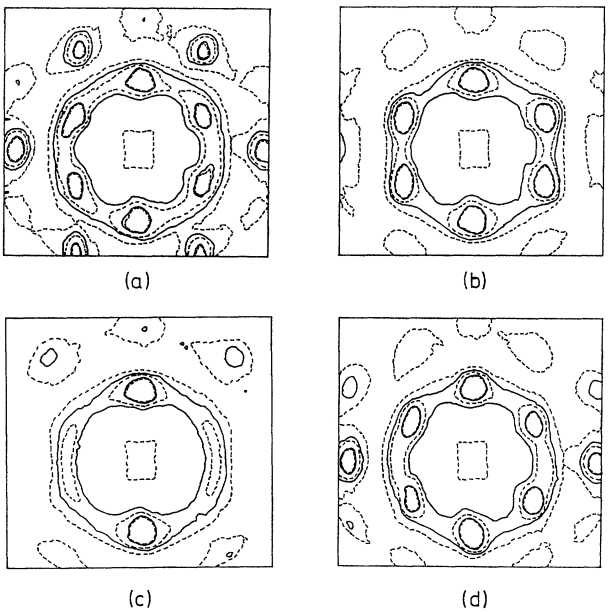

FIG. 4. Small-angle neutron scattering pattern from a charge stabilized dispersion flowing in the $(\bar{2}, 1)$-$(0, 0)$-$(2, \bar{1})$ direction with a wall shear rate of 10^{-4} s^{-1}, redrawn after Ref. [7], Fig. 21. Indexing is as in Fig. 3(a). (a) Neutron beam at normal incidence on the layers. (b) Sample rotated by 30°, and (c) sample rotated by 45° about the vertical (0,1)-(0,0)-$(0, \bar{1})$ axis. (d) Sample rotated by 22.5° about the horizontal $(\bar{2}, 1)$-$(0, 0)$-$(2, \bar{1})$ axis.

Further information concerning the intensity distribution on the Bragg rods can be obtained from the orientation dependence of the scattering pattern. Figures 4(b) and 4(c) show how the intensity distribution changes as the cell is rotated about the vertical (0,1)-(0,0)-$(0, \bar{1})$ axis by 30° and by 45°, respectively. Such a rotation causes the Ewald plane to rotate in the reciprocal lattice, as indicated in Fig. 3(b), by the two rotated lines (projections of the Ewald plane). The Ewald plane now intersects the rods at different l values, i.e., changing the orientation of the sample allows one to scan the intensity along the Bragg rods.

Let us consider the $(h - k) = 3n$ rods shown on the right-hand side of Fig. 3(b) first. For a rotation by 30° the Ewald plane intersects the rods (1,1), $(1, \bar{2})$, and $(\bar{1}, \bar{1})$, $(\bar{1}, 2)$ at $l \approx \pm\frac{1}{2}$, where for close-packed hexagonal planes the intensity should be zero. In fact, a strong decrease of the intensity is observed in Fig. 4(b) for these reflections. Further rotation to 45° brings the Ewald plane closer to the next nodes ($l = \pm 1$) on these rods and, accordingly, a slight increase of the intensity is visible in Fig. 4(c). Further, the position of the Bragg peaks as a function of the sample orientation can be understood. Peaks on the (0,1)-(0,0)-$(0, \bar{1})$ rotation axis are independent of the sample orientation because the Ewald plane intersects these rods at $l = 0$. For rods not intersecting the rotation axis the intensity "moves away" from the rotation axis as the sample is rotated. The distance d^* of a (h, k) reflection from the rotation axis is $d^*(\theta) = \sqrt{3}a^*|h|/2 \cos(\theta)$, where θ is the rotation angle. For example, the reflections $(\bar{2}, 1)$ and $(2, \bar{1})$, which are visible in Fig. 4(a), are moved outward in Fig. 4(b) and are no longer visible in Fig. 4(c); similarly, the reflections (1,1) and $(\bar{1}, 2)$ drift apart with rotation angle.

Next, the $(h - k) = 3n \pm 1$ rods are considered. Rotation of the cell by 30° has two effects for the rods not intersecting the rotation axis: $(\bar{1}, 1)$, (1,0) and $(\bar{1}, 0)$, $(1, \bar{1})$. They move apart as discussed before and gain somewhat in intensity. Since the Ewald plane intersects the Bragg rods at $l \approx \pm\frac{1}{2}$, the intensity distribution for random close packing with its maxima at $l = \pm\frac{1}{2}$ [shown on the left-hand side of Fig. 3(b)] is favored by this finding. According to Fig. 4(c) further rotation of the cell to 45° leads to a total vanishing of the latter spots. As the intersection of the Ewald plane with the $(\bar{1}, k)$-Bragg rods in Fig. 3(b) shows, the intensity should not vanish com-

pletely for random packing. This could be an indication that the stacking order may be closer to hcp with stacking faults, for which, according to Fig. 2, upper panel, a minimum of $I(l)$ occurs in this l range.

The scattering pattern shown in Fig. 4(d) was obtained after rotating the cell from the normal position about the horizontal $(\bar{2},1)$-$(0,0)$-$(2,\bar{1})$ axis by 22.5°. The intersections of the Bragg rods by the rotated Ewald plane are shown in Fig. 3(c). First, the intensity of the $(h-k)=3n$ nodes on the rotation axis $(\bar{2},1)$ and $(2,\bar{1})$ neither move nor change their intensity. By contrast, the $(h-k)=3n$ nodes not on the rotation axis [(1,1), $(\bar{1},2)$, and $(1,\bar{2})$, $(\bar{1},\bar{1})$] drastically lose intensity, in agreement with the fact that the Ewald plane intersects the corresponding Bragg rods at $l \approx \frac{1}{2}$. Second, concerning the $(h-k)=3n \pm 1$ rods the intensity of the reflections (1,0), $(\bar{1},1)$ and $(1,\bar{1})$, $(\bar{1},0)$ changes little as compared with the one in Fig. 4(a), whereas the reflections (0,1) and $(0,\bar{1})$ have gained intensity. The intensity distribution for random packing shown in the lower part of Fig. 3(c) perfectly accounts for this behavior. The Ewald sphere intersects the $(1,\bar{1})$, $(\bar{1},0)$ and symmetrically the (1,0), $(\bar{1},1)$ rods in a region in which $I(l)$ is still close to its value at $l=0$. The intersection of the (0,1), $(0,\bar{1})$ rods, on the other hand, occurs closer to the maxima at $l=\pm\frac{1}{2}$ of the $I(l)$ distribution. The slight shift of the peaks also perfectly fits into the Bragg rod picture.

For rotations of the sample about the vertical axis the rotation angle θ_v is related to the l value at which a (h,k) rod is intersected by the Ewald plane by $\tan(\theta_v) = (3/2)^{1/2} l/h$. In order to distinguish between the different possible stacking sequences intensity measurements at $l=0$, $\frac{1}{3}$, $\frac{1}{2}$, $\frac{2}{3}$, and l would be of particular interest. For the (1,0) rod the corresponding sample orientations are $\theta_v = 0°$, 22.2°, 31.48°, 39.32°, and 50.77°. Unfortunately, measurements at these angles are not available. For rotations about the horizontal axis the relation $\tan(\theta_h) = (3/\sqrt{2})l/s$ holds, where s is the rod index corresponding to the projection shown in Fig. 3(c).

In conclusion, we have shown that for a shear ordered system at low shear rate the neutron scattering distribution and its orientation dependence can be accounted for qualitatively in terms of the intensity distribution $I(l)$ along the Bragg rods. The structure of the system considered is close to random close-packed hexagonal layers. The method of analysis appears suited to study the structure of sheared samples and the kinetics of recrystallization quantitatively. Such investigations require a continuous variation of the sample orientation which does not seem to be available at the moment.

Financial support of the Deutsche Forschungsgemeinschaft and the Fonds der Chemischen Industrie is gratefully acknowledged.

[1] P. N. Pusey, *In Liquids, Freezing and the Glass Transition,* edited by D. Levesque, J.-P. Hansen, and J. Zinn-Justin (North-Holland, Amsterdam, 1991).
[2] E. B. Sirota, H. D. Ou-Yang, S. K. Sinha, P. M. Chaikin, J. D. Axe, and Y. Fujii, Phys. Rev. Lett. **62**, 1524 (1989).
[3] Z. Monovoukas and A. P. Gast, J. Colloid. Interface Sci. **128**, 533 (1989).
[4] M. O. Robbins, K. Kremer, and G. S. Grest, J. Chem. Phys. **88**, 3286 (1988).
[5] B. J. Ackerson, J. B. Hayter, N. A. Clark, and L. Cotter, J. Chem. Phys. **84**, 2344 (1986).
[6] S. Ashdown, I. Markovic, R. H. Ottewill, P. Lindner, R. C. Oberthür, and A. R. Rennie, Langmuir **6**, 303 (1990).
[7] H. M. Laun, R. Bung, S. Hess, W. Loose, O. Hess, K. Hahn, E. Hädicke, R. Hingmann, F. Schmidt, and P. Lindner, J. Rheol. **36**, 743 (1992).
[8] M. Joanicot, K. Wong, J. Maquet, Y. Chevalier, C. Pichot, C. Graillat, P. Lindner, L. Rios, and B. Cabane, Prog. Colloid Polym. Sci. **81**, 175 (1990).
[9] H. Versmold and H. P. Lindner, Langmuir **10**, 3043 (1994).
[10] P. N. Pusey, W. van Megen, P. Bartlett, B. J. Ackerson, J. G. Rarity, and S. M. Underwood, Phys. Rev. Lett. **63**, 2753 (1989).
[11] A. Guinier, *X-Ray Diffraction* (Freeman, London, 1963).